Frontiers in Bioscience Landmark

Front. Biosci. (Landmark Ed) **2025**; 30(8): 27946
https://doi.org/10.31083/FBL27946

Original Research

Knockdown of ITGA2 Promotes Pyroptosis in Thyroid Cancer by Regulating the DNA Damage Response

Liang Yan[1,†], Dongming Hua[2,†], Rong Ying[2], Xiaoshuang Liu[1], Jun Jiang[3], Zhaolong Liu[1,*], Yu Feng[4,*]

[1]Thyroid Surgery, Shanghai University of Traditional Chinese Medicine Affiliated Shuguang Hospital, 201203 Shanghai, China
[2]Department of Medical Oncology, Shanghai University of Traditional Chinese Medicine Affiliated Shuguang Hospital, 201203 Shanghai, China
[3]Endoscopy Center, Minhang Hospital, Fudan University, 201100 Shanghai, China
[4]General Surgery, Shanghai Pudong New District Traditional Chinese Medicine Hospital, 200120 Shanghai, China
*Correspondence: liuzhaolong7677@126.com (Zhaolong Liu); davisfy@126.com (Yu Feng)
[†]These authors contributed equally.

Academic Editor: Amedeo Amedei
Submitted: 6 November 2024 Revised: 27 May 2025 Accepted: 9 June 2025 Published: 18 August 2025

Abstract

Background: The most common endocrine cancer, thyroid carcinoma (TC), has a dismal prognosis when it reaches an advanced stage. Integrin α-2 (*ITGA2*) has been implicated in cancer progression, influencing both DNA damage and repair mechanisms. However, it is unknown how ITGA2 influences these processes in TC. **Methods**: *ITGA2* was identified as a key prognostic gene for TC from the Cancer Genome Atlas-thyroid carcinoma (THCA), GSE3678, GSE29265, and GSE33630 datasets. Functional assays were used to evaluate the impact of *ITGA2* knockdown on cell viability, migration, apoptosis, invasion, pyroptosis (N-terminal fragment of GSDME, GSDME-N), and cytotoxicity (Lactate dehydrogenase, LDH). DNA damage markers (phosphorylated histone H2AX on serine 139 (γ-H2AX), phosphorylated ataxia telangiectasia mutated (p-ATM), phosphorylated checkpoint kinase 2 (p-CHK2)) and the level of Reactive Oxygen Species (ROS) were used to assess oxidative stress. The impact of *ITGA2* inhibition on Wnt/β-catenin signaling was evaluated, and a mouse xenograft model assessed tumor growth *in vivo*. **Results**: *ITGA2* was significantly overexpressed in TC. Knockdown of *ITGA2* significantly reduced cell viability, migration, and invasion, while promoting pyroptosis by upregulating cleaved-poly(ADP-ribose) polymerase (PARP) and GSDME-N. *ITGA2* silencing also increased LDH activity, enhanced the expression of DNA damage markers (p-ATM, γ-H2AX, p-CHK2), and increased ROS levels. Furthermore, suppression of *ITGA2* activity attenuated the Wnt/β-catenin pathway by reducing the levels of MYC proto-oncogene, bHLH transcription factor (C-myc), CD44 molecule (CD44), slug, snail, β-catenin, and wingless-type MMTV integration site family, member 1 (Wnt-1). *ITGA2* silencing significantly inhibited tumor growth in a mouse model. **Conclusion**: *ITGA2* promotes TC progression by regulating the DNA damage response and inhibiting pyroptosis. Knockdown of *ITGA2* increases oxidative stress, exacerbates DNA damage, and inhibits the Wnt/β-catenin pathway, indicating it may have potential as a treatment target in TC.

Keywords: thyroid cancer; *ITGA2*; Wnt/β-catenin signaling pathway; DNA damage; pyroptosis

1. Introduction

Thyroid cancer (TC) is the most common endocrine malignancy globally and shows an increasing incidence [1]. Early intervention and the use of various therapeutic approaches, including surgical procedures, radioactive iodine treatment, and thyroid hormone therapy, have improved the outcomes for many TC patients. Patients with advanced or metastatic illness, on the other hand, continue to face bleak prospects [2]. DNA damage is pivotal in TC progression due to its activation of critical pathways, such as pyroptosis and apoptosis [3]. Apoptosis is a non-inflammatory, programmed mode of cellular demise, whereas pyroptosis is a pro-inflammatory process that entails inflammasome activation and the cleavage of gastrin [4,5]. Minor DNA damage can be repaired, but severe or persistent damage triggers cell death pathways [6]. The pro-inflammatory effects of pyroptosis may contribute to the aggressive behavior of specific TC subtypes [7]. Therefore, it is essential to comprehend the connection between DNA damage and cell death in TC in order to create innovative treatment approaches [8].

Integrin alpha-2 (*ITGA2*) is a transmembrane receptor that forms the $\alpha 2\beta 1$ integrin complex. Recent data also indicates that *ITGA2* is essential in the DNA damage response. Specifically, the overexpression of *ITGA2* negatively affects the process of DNA repair, primarily by interfering with the non-homologous end-joining (NHEJ) mechanism, which is crucial for the repair of double-strand DNA breaks [9]. This disruption increases genomic instability and sensitizes tumor cells to treatments such as radiotherapy. Zhou *et al.* [10] showed that *ITGA2* overexpression in pancreatic cancer exacerbates DNA damage and enhances radiation sensitivity. The Wnt/β-catenin signaling cascade is a well-known regulator of cell proliferation, differentia-

tion, and stem cell maintenance. This pathway has attracted significant attention for its potential involvement in facilitating DNA repair mechanisms [11]. Dysregulation of the Wnt/β-catenin pathway inhibits cellular repair systems, increasing genomic instability [12]. *ITGA2* may influence cancer progression by directly impairing DNA repair and connecting with the Wnt/β-catenin signaling pathway. In hepatocellular carcinoma, the transcription factor *TCF7L1* modulates *ITGA2* expression, thereby establishing a direct connection to the Wnt/β-catenin signaling axis and influencing tumorigenic processes such as expansion and dissemination [13].

ITGA2 plays a complex function in cancer development. This includes the disruption of DNA repair processes, enhancement of genomic instability, and stimulation of cancer-promoting pathways like Wnt/β-catenin. Targeting of *ITGA2* could therefore be a promising therapeutic strategy for cancers with aberrant DNA damage response and signaling pathways, including TC. This study aimed to investigate the function of *ITGA2* in TC by integrating a bioinformatics analysis with functional assays. To further understand the molecular pathways underlying TC advancement, we investigated the impact of *ITGA2* knockdown on tumor cell behavior, pyroptosis, as well as DNA damage response.

2. Materials and Methods

2.1 Extraction and Analysis of TC Data

Three TC datasets (GSE29265, GSE3678, GSE33630) were collected from the Gene Expression Omnibus database (GEO; https://www.ncbi.nlm.nih.gov/gds/). The GSE3678 dataset comprises 7 TC samples and 7 paired control samples, the GSE29265 dataset contains 29 TC samples and 20 control samples, while the GSE33630 dataset contains 60 TC samples and 45 control samples. Furthermore, information collected The Cancer Genome Atlas (TCGA; https://portal.gdc.cancer.gov/) database, which included 59 control samples and 512 TC samples, was also used. To identify differentially expressed genes (DEGs) in the datasets, the ASSISTANT for Clinical Bioinformatic platform (https://www.aclbi.com/static/index.html#/) was utilized. A fold-change (FC) threshold of >2 indicated upregulation of DEGs, whereas a FC threshold of <0.5 indicated downregulation of DEGs. The criterion for statistical significance was set at a p-value of less than 0.05.

2.2 Identification of Overlapping DEGs and Building Protein-Protein Interaction (PPI) Networks

Overlapping DEGs from the four TC datasets were identified using a bioinformatics platform (https://bioinformatics.psb.ugent.be/webtools/Venn/). Intersection analysis of both upregulated and downregulated DEGs was used to obtain DEGs that overlapped. The Search Tool for the Retrieval of Interacting Genes/Proteins (STRING) database (https://string-db.org/) was used to identify PPI networks among overlapping DEGs. Further exploration of potential functional associations and regulatory networks of candidate genes was carried out by constructing PPI networks. Analysis was performed using the Molecular Complex Detection (MCODE) algorithm. For visualization, the Cytoscape open-source software platform (version 3.7.1; Cytoscape Consortium, San Diego, CA, USA) was applied to the resulting PPI network.

2.3 Building of a Predictive Model and Analysis of Survival Using LASSO Regression of the Overlapping DEGs

Overlapping DEGs were analyzed with the "glmnet" package in R software. Tuning parameters were determined through a 10-fold cross-validation process, and the Least Absolute Shrinkage and Selection Operator (LASSO) model was applied [14–16]. To find the most predictive genes, we employed the ideal λ, which represents the minimal adjusted parameter criteria. These formed the basis of the predictive model. To find the most predictive genes, we employed the ideal λ, which represents the minimal adjusted parameter criteria. Kaplan-Meier (KM) analysis estimated overall survival (OS) probabilities, and the log-rank test evaluated differences between survival curves. To evaluate relative risk, the hazard ratio (HR) for the high-risk group was computed [17]. The "timeROC" tool was used to generate receiver operating characteristic (ROC) curves, and the area under the curve [18] was calculated to determine how well the model predicted one-, three-, and five-year survival rates. Higher area under the curve (AUC) values showed improved prediction accuracy.

2.4 Analysis of Prognostic Genes, and Nomogram Construction for Survival Prediction

Correlation analysis for significant prognostic genes was performed using R software. Single-factor and multifactor Cox regression analyses were conducted on signature genes and clinical variables (age, gender, pathological TNM (pTNM) stage) using the "forest plot" package. For each variable, the 95% confidence intervals (CIs) [19], p-values, and HRs were computed. Statistically significant variables ($p < 0.05$) in survival analysis were found as crucial prognostic factors. The "regression modeling strategies (RMS)" program was used to create nomograms that predicted the probability of one-, three-, and five-year survival. The concordance index was calculated to assess model accuracy. Calibration curves were generated, and the closer the alignment of the survival prediction curve to the calibration curve, the better the model performance. Gene expression levels were evaluated using R and visualized with boxplots to compare tumor and paired control groups from the TCGA-thyroid carcinoma (THCA), GSE3678, GSE29265, and GSE33630 datasets.

2.5 Cell Lines and Culture

Otwo Biotech (Shenzhen, China) provided the normal thyroid cell line (Nthy-ori3-1), the TC cell line TPC-1, and CAL-62. The selection of TPC-1 (papillary carcinoma) and CAL-62 (mesenchymal carcinoma) was based on the unequivocal identification of their molecular features in a previous study [20] and is widely used in studies of thyroid cancer migration, DNA damage, and cell death [21]. The two cell lines can be studied to cover the heterogeneity of the main subtypes of thyroid cancer. In a humidified 37 °C atmosphere with 5% CO_2, cells were cultivated in Dulbecco's Modified Eagle Medium (DMEM; Procell; cat. no. PM150210B; Wuhan, China) supplemented with 10% fetal bovine serum (FBS) (Gibco; Thermo Fisher Scientific, Inc.; cat. no. 16000044; Waltham, MA, USA) and 1% penicillin-streptomycin (Beyotime; cat. no. C0222; Shanghai, China). We declare that all cell lines used in this study tested for mycoplasma contamination using PCR-based detection methods, and were confirmed to be free of contamination (**Supplementary Fig. 1**). All cell lines were obtained from OTWO (Huatuo Biotech, China). The supplier verified the authenticity of these cell lines using short tandem repeat (STR) profiling.

2.6 Cell Transfection

To conduct transient transfection, TC cells were seeded in 24-well plates at a density of 2×10^5 per well. *ITGA2* was knocked down utilizing two different small interfering RNAs (siRNAs) that target it. Lipofectamine 3000 (Invitrogen; Thermo Fisher Scientific, Inc.; cat. no. L3000150; MA, USA) was used to transfect TC cells for a given period of time, as indicated by the manufacturer. si-*ITGA2* siRNA sequence information: si-*ITGA2*-1: 5′-UUCUCAGGAAAGCCACUCCAGGGUG-3′ (Sense Sequence), 5′-UUCUCAGCAGAAGGCCACUCCAG-3′ (Antisense Sequence); si-*ITGA2*-2, 5′-GAGCCUUUAGGAGCCAUCUCCAGUA-3′, 5′-UACUGGAGAUGGCUCCUAAAGGCUC-3′ (Antisense Sequence); si-NC (non-targeting control) siRNA sequences: 5′-CACAGGUGGUGUUUCGUCCACCGAA-3′ (Sense Sequence), 5′-UUCGGUGGACGAAACACCACCUGUG-3′ (Antisense Sequence).

2.7 Quantitative Real-time Polymerase Chain Reaction (qRT-PCR)

qRT-PCR was carried out as previously mentioned [22]. The relative expression of genes was determined using the $2^{-\Delta\Delta CT}$ technique, and the levels were normalized to glyceraldehyde-3-phosphate dehydrogenase (*GAPDH*). The primer sequences utilized in the qRT-PCR tests are listed in Table 1.

2.8 Western Blot (WB) Assay

To extract protein lysates from TC cells, a combination of protease inhibitor cocktail (CoWin Biosciences; cat. no. CW2200S; Nanjing, China) and phosphatase inhibitors cocktail (CoWin Biosciences; cat. no. CW2383S; Nanjing, China) was combined with RIPA lysis solution (Solarbio; cat. no. R0020; Beijing, China). Before the protein was separated using 10% SDS-PAGE and then transferred onto PVDF membranes (Beyotime; cat. no. FFP22; Beijing, China), the protein concentration was measured using a BCA Protein Assay Kit (Beyotime; cat. no. P0012; Beijing, China). Primary antibodies were then administered overnight at 4 °C after the membranes had been blocked for an hour at room temperature using 5% skim milk. These included antibodies to ITGA2 (cat. no. ab181548), BCL2-associated X protein (Bax) (cat. no. ab32503), caspase-3 (cat. no. ab32351), caspase-9 (cat. no. ab32539), BCL2 apoptosis regulator (Bcl-2) (cat. no. ab182858), poly(ADP-ribose) polymerase (PARP) (cat. no. ab191217), cleaved-PARP (cat. no. ab32561), GSDME-full length (GSDME-FL) (cat. no.

Table 1. Primer sequences for qRT-PCR.

Target	Direction	Sequence (5′-3′)
ITGA2	Forward	TTCAGCTCTCAGCCAGCTTC
ITGA2	Reverse	ACCCCACCTGTGTCTTTGTG
Bax	Forward	TGATGGACGGGTCCGGG
Bax	Reverse	TGAGACACTCGCTCAGCTTC
Caspase3	Forward	TGTGAGGCGGTTGTAGAAGAGT
Caspase3	Reverse	CTTTATTAACGAAAACCAGAGCGCC
Caspase9	Forward	GGCCCCATATGATCGAGGAC
Caspase9	Reverse	CAACTTTGCTGCTTGCCTGT
Bcl-2	Forward	AAAAATACAACATCACAGAGGAAGT
Bcl-2	Reverse	AGGGGGTGTCTTCAATCACG
Wnt-1	Forward	TGTGGAAATGAGGTTGGGGG
Wnt-1	Reverse	CGTGGCTCTGTATCCACGTT
C-myc	Forward	ACACTAACATCCCACGCTCTG
C-myc	Reverse	AAATCATCGCAGGCGGAACA
CD44	Forward	GAGCAGCACTTCAGGAGGTT
CD44	Reverse	TGGTTGCTGTCTCAGTTGCT
β-catenin	Forward	GTTGAGCACCTGTTTGCCTG
β-catenin	Reverse	GTTGAGCACCTGTTTGCCTG
Slug	Forward	CATCTTTGGGGCGAGTGAGT
Slug	Reverse	GGCCAGCCCAGAAAAAGTTG
Snail	Forward	CGAGTGGTTCTTCTGCGCTA
Snail	Reverse	GGGCTGCTGGAAGGTAAACT
GAPDH	Forward	AATGGGCAGCCGTTAGGAAA
GAPDH	Reverse	GCGCCCAATACGACCAAATC

qRT-PCR, quantitative real-time polymerase chain reaction; *ITGA2*, Integrin α-2; *Bax*, BCL2-associated X protein; *Bcl-2*, BCL2 apoptosis regulator; *Wnt-1*, wingless-type MMTV integration site family, member 1; *C-myc*, MYC proto-oncogene; bHLH transcription factor; *GAPDH*, glyceraldehyde-3-phosphate dehydrogenase.

ab215191), N-terminal fragment of GSDME (GSDME-N) (cat. no. ab222408), phosphorylated histone H2AX on serine 139 (γ-H2AX) (cat. no. ab81299), MYC proto-oncogene, bHLH transcription factor (C-myc) (cat. no. ab32072), CD44 molecule (CD44) (cat. no. ab51037), β-catenin (cat. no. ab32572), slug (cat. no. ab51772), snail (cat. no. ab216347), phosphorylated checkpoint kinase 2 (p-CHK2) (cat. no. ab85743), and phosphorylated ataxia telangiectasia mutated (p-ATM) (cat. no. ab36810) (Abcam; Cambridge, UK; 1:1000), as well as wingless-type MMTV integration site family, member 1 (Wnt-1) (Wuhan Sanying; cat. no. 27935-1-AP; Wuhan, China; 1:1000). Following membrane washing, the proper secondary antibodies (Kangcheng; cat. no. KC-RB-035; Shanghai, China; 1:5000) were added. The protein bands were seen using an enhanced chemiluminescence kit (Tiangen; cat. no. PA110; Beijing, China), and the data were recorded and analyzed using the ChemiDoc Imaging System (Bio-Rad, Shanghai, China). The loading control was GAPDH (Abcam; cat. no. ab8245; 1:1000).

2.9 Cell Counting Kit-8 (CCK-8) Assay

The CCK-8 analysis method (KeyGEN; cat. no. KGA317; Nanjing, China) was used to assess cell viability. At a density of 5×10^3 cells per well, TC cells were seeded onto 96-well plates. A microplate reader (Kehua Technologies, Shanghai, China) was used to measure the absorbance at 450 nm after the CCK-8 reagent was added to each well at 0, 1, 2, 3, 4, and 5 days.

2.10 Flow Cytometry

Trypsin-EDTA (Absin; cat. no. abs42104714; Shanghai, China) was used to separate TC cells, and then washing with phosphate-buffered saline (PBS; Beyotime; cat. no. C0221B; Shanghai, China). As advised by the manufacturer, the cells were labeled with Annexin V (BD Biosciences; cat. no. 563973; San Jose, CA, USA) and propidium iodide (PI) (BD Biosciences; cat. no. 556547; San Jose, CA, USA). Viable, necrotic, and apoptotic cells were then separated using a flow cytometer (Jiyuan, Guangzhou, China). FlowJo software (version 7.6, FlowJo, Hangzhou, China) was utilized for processing the flow cytometry data.

2.11 Transwell Assays

Transwells were utilized to monitor cell invasion and migration. Transfected TC cells were placed in serum-free media in the top compartment of the Transwell instrument.

Subsequently, the medium in the lower compartment was enriched with 10% FBS. After a 24-hour incubation period, the cells were fixed with 4% paraformaldehyde (Wuhan Servicebio Biotechnology Co., Ltd.; cat. no. G1101; Wuhan, China) and stained with DAPI (Abcam; cat. no. ab104139; Cambridge, UK). The migration of cells into the bottom compartment was then assessed using inverted microscopy. The upper chamber was initially covered with matrigel for the cell invasion studies, and the same steps as for cell migration were taken.

2.12 Enzyme-linked Immunosorbent Assay (ELISA)

A suitably diluted quantity of cell culture supernatant was then added to the wells of ELISA plates that had previously been coated with IL-1β antibodies (Wuhan Sanying; cat. no. 16806-1-AP; Wuhan, China). The chromogenic substrate was added after the enzyme-linked secondary antibody had been incubated and cleaned. The reaction was subsequently terminated and absorbance at the specified wavelength was measured using a microplate reader. The absorbance results were compared to a standard curve created with known quantities of IL-1β in order to ascertain the amount of IL-1β present in each sample.

2.13 Xenograft Model

To create the xenograft model, TC cells transfected with si-NC and si-*ITGA2*-1 were suspended in serum-free media. Subcutaneous injections of a 100 µL solution containing 5×10^6 cells were then administered to the flanks of ten 6-week-old female BALB/c nude mice (n = 3 per group). Subsequently, calipers were used to measure the tumor dimensions every week for 28 days. The formula used to compute the tumor volume was $0.52 \times \text{length} \times \text{width}^2$. An intraperitoneal dose of sodium pentobarbital (150 mg/kg, 50 mg/mL) was administered to euthanize the animals after 4 weeks. Tumors were then surgically excised, weighed, and analyzed histologically. All animal procedures were approved by the Animal Welfare and Ethics Committee of the Laboratory Animal Science Department, Fudan University (No. 2024-MHYY-304), and were conducted following institutional ethical guidelines and complied with the 3R (Replacement, Reduction, Refinement) principles.

2.14 Biochemical Assays for Oxidative Stress and Cytotoxicity Markers

Lactate dehydrogenase (LDH; cat. no. P0395S) activity and reactive oxygen species (ROS; cat. no. S0035) levels were assessed following the manufacturer's instructions. The corresponding detection kits were used, respectively (Beyotime Institute of Biotechnology, Jiangsu, China).

2.15 Immunohistochemistry

After embedding the subcutaneous tumor tissues of mice in sections as required, the oven temperature was set to 65 °C and baked at a constant temperature for 120 mins. This was performed according to the immunohistochemistry kit (Maxim; cat. no. Kit9710; Fuzhou, China). Sections were incubated with an anti-ITGA2 primary antibody (Abcam, cat. no. ab181548; 1:500 dilution) overnight at 4 °C, followed by detection using the HRP-conjugated secondary antibody (Kangcheng; cat. no. KC-RB-035; 1:250 dilution, Shanghai, China). The complete tissue sample

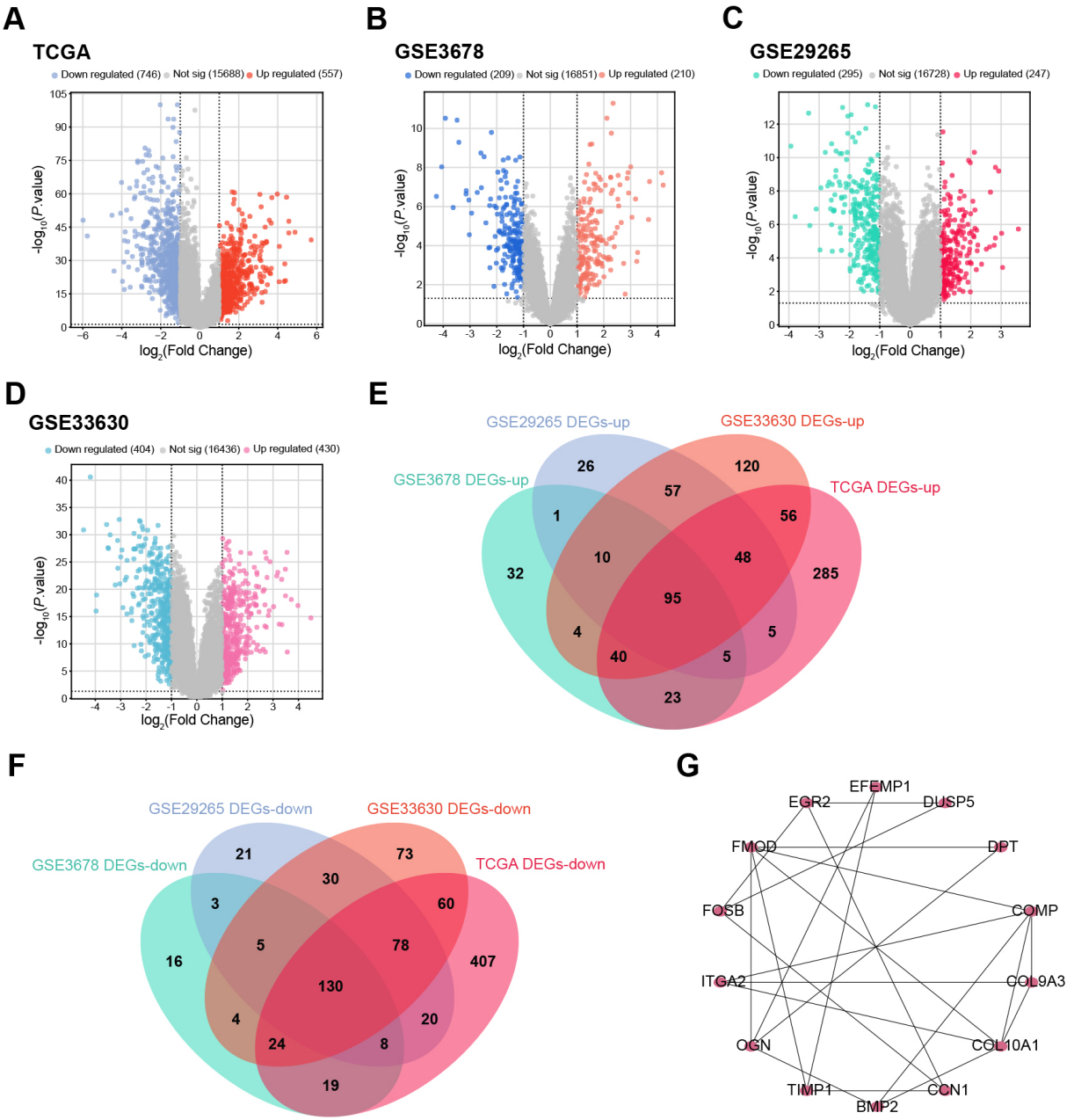

Fig. 1. Construction of the PPI network for DEGs identified in the TC datasets. (A–D) Volcano plots showing DEGs in TCGA-THCA (A), GSE3678 (B), GSE29265 (C), and GSE33630 (D) datasets. Red dots represent up-regulated DEGs, and blue dots represent down-regulated DEGs. Grey dots indicate non-significant genes. A *p*-value of <0.05 was the threshold for statistical significance. (E,F) Venn diagram showing the overlap of up-regulated DEGs (E) and down-regulated DEGs (F) in the four datasets. The number in each segment indicates the number of shared genes. (G) The MCODE algorithm revealed the PPI network of overlapping genes, which contained 14 nodes and 23 edges. Node size corresponds to degree of interaction, and edge thickness represents interaction confidence. PPI, protein-protein interaction; TCGA, The Cancer Genome Atlas; DEGs, differentially expressed genes; THCA, thyroid carcinoma; MCODE, Molecular Complex Detection; TC, thyroid carcinoma.

was scanned at low magnification (×10) to evaluate staining, and it was verified at high magnification (×20).

2.16 Statistical Analysis

Data was analyzed using the R program (version 4.2.2, R Foundation for Statistical Computing, Vienna, Austria). Three duplicates of each experiment were conducted, and the mean ± standard deviation (SD) was used to report the data. Tukey's post-hoc test was used for pairwise comparisons after one-way ANOVA was used for multi-group comparisons. Statistical significance was defined as a *p*-value of less than 0.05.

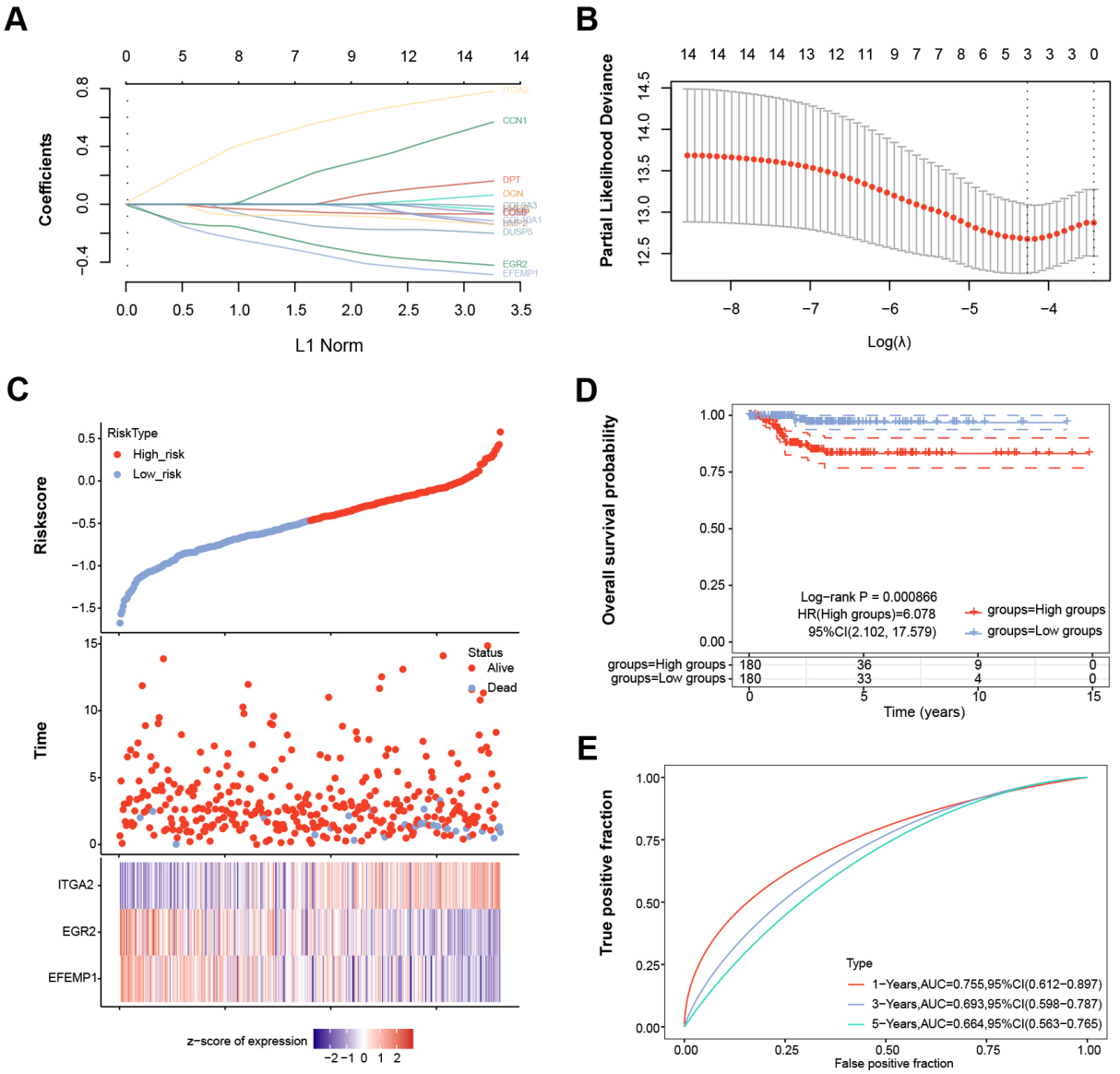

Fig. 2. LASSO Cox regression and survival analysis for three key prognostic genes in TC. (A) LASSO coefficient profiles of 14 candidate genes. Each curve represents the relationship between the gene coefficient and the L1 norm. The optimal lambda value was determined by minimizing the partial likelihood deviation. (B) Plot of the correlation between log(λ) and 10-fold cross-validated partial likelihood deviation for selecting the best λ value. (C) Risk model analysis of the selected sample data. The upper panel displays the risk scores, the middle panel shows survival status (red dots indicate high-risk, blue dots indicate low-risk), and the lower panel is a heatmap of the clustering distribution of the three critical genes (*ITGA2*, *EGR2*, *EFEMP1*). (D) KM survival curves for the two risk-model-identified groups. The log-rank test was used to assess differences in survival probability, with a *p*-value of 0.000866 and a HR of 6.078 for high-risk groups compared to low-risk groups. (E) ROC curve for the patient risk model after 1, 3, and 5 years of follow-up. The real positive score is shown on the vertical axis, while the false positive score is shown on the horizontal axis. The AUC values are provided for each time point, indicating the model's predictive accuracy. TC, thyroid carcinoma; LASSO, Least Absolute Shrinkage and Selection Operator; DEGs, differentially expressed genes; ROC, Receiver Operating Characteristic; KM, Kaplan-Meier; AUC, Area Under the Curve; HR, Hazard Ratio; CI, Confidence Interval.

3. Results

3.1 Identification of DEGs in TC, and Construction of the PPI Network

The number of up-regulated DEGs found in the TCGA-THCA, GSE3678, GSE29265 and GSE33630 datasets was 557, 210, 247 and 430, respectively, while the number of down-regulated DEGs was 746, 209, 295 and 404, respectively (Fig. 1A–D). An integrated bioinformatics platform found that 95 up-regulated DEGs as well as 130 down-regulated DEGs overlapped across all four datasets

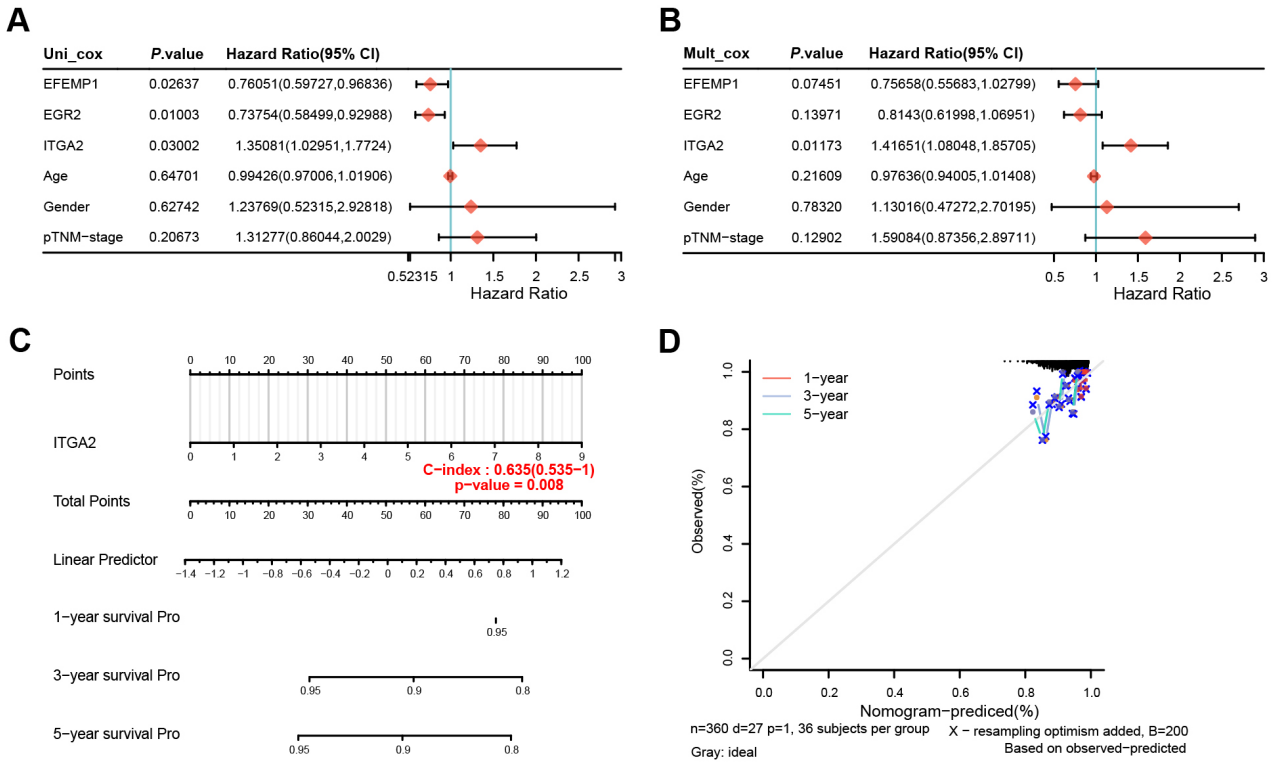

Fig. 3. Survival analysis and prognostic assessment in TC. (A) Univariate Cox regression analysis of clinical prognostic factors and critical genes for TC patient survival. The forest plot displays HRs with 95% CI and *p*-values for each variable. (B) Multivariate Cox regression analysis of the same factors, adjusting for potential confounders. The forest plot shows adjusted HRs with 95% CI and *p*-values. (C) Nomogram for predicting 1-year, 3-year, and 5-year survival probabilities based on key prognostic factors (*ITGA2*, Age, Gender, pTNM-stage). The total points for each factor are summed to obtain a linear predictor, which is then translated into survival probabilities. The model's predictive accuracy is assessed using the C-index, with a value of 0.635 (95% CI: 0.535–1) and a *p*-value of 0.008. (D) Calibration plot for the nomogram, showing observed versus predicted survival probabilities at 1-year, 3-year, and 5-year follow-ups. The dashed lines represent ideal prediction, while the solid lines show the actual performance of the model. The calibration plot was generated using the Clinical Bioinformatics Platform. The clustering of observed points in the upper-right region reflects the high survival probability in our TC cohort. TC, Thyroid Carcinoma; Cox, Cox proportional hazards model; HR, Hazard Ratio; CI, Confidence Interval; C-index, Concordance Index.

(Fig. 1E,F). Further analysis of these overlapping DEGs was performed by constructing a PPI network. This identified 14 genes using the MCODE plugin (Fig. 1G).

3.2 Analysis of Three Critical Prognostic Genes in TC

As shown in Fig. 2A,B, three critical prognostic genes were identified from the 14 genes based on the ideal lambda value (λmin = 0.014), giving the following risk score: (–0.1389) × *EFEMP1* + (–0.1195) × *EGR2* + (–0.2028) × *ITGA2*. In terms of mortality and survival, the high-risk group did better than the low-risk group (Fig. 2C). Survival analysis of these 3 genes using the KM method showed a significantly lower OS in the high-risk group, with an HR of 6.078 (>1) (Fig. 2D). Additionally, ROC curve analysis showed the predictive ability of this model was strongest at one year of follow-up, with an area under the curve (AUC) of 0.755 (Fig. 2E).

3.3 Association Analysis of ITGA2 Gene Expression and Prognosis of Thyroid Cancer Patients

Cox regression analysis and survival analysis of key prognostic factors in TC patients. The results of univariate Cox regression analysis for the 3 key candidate genes (*EFEMP1*, *EGR2*, and *ITGA2*) showed significant prognostic correlations, indicating that the expression levels of these genes were significantly correlated with the survival prognosis of patients (Fig. 3A). After adjusting for potential confounders, the results of multivariate Cox regression analysis for the 3 key candidate genes indicated that the *ITGA2* gene still showed a significant prognostic correlation, suggesting that *ITGA2* may be an independent prognostic factor (Fig. 3B). The column-line graph demonstrated a prognostic model constructed based on *ITGA2* expression levels and other clinicopathologic features (Fig. 3C). The analysis showed that the predictive ability of the model was statistically significant. The calibra-

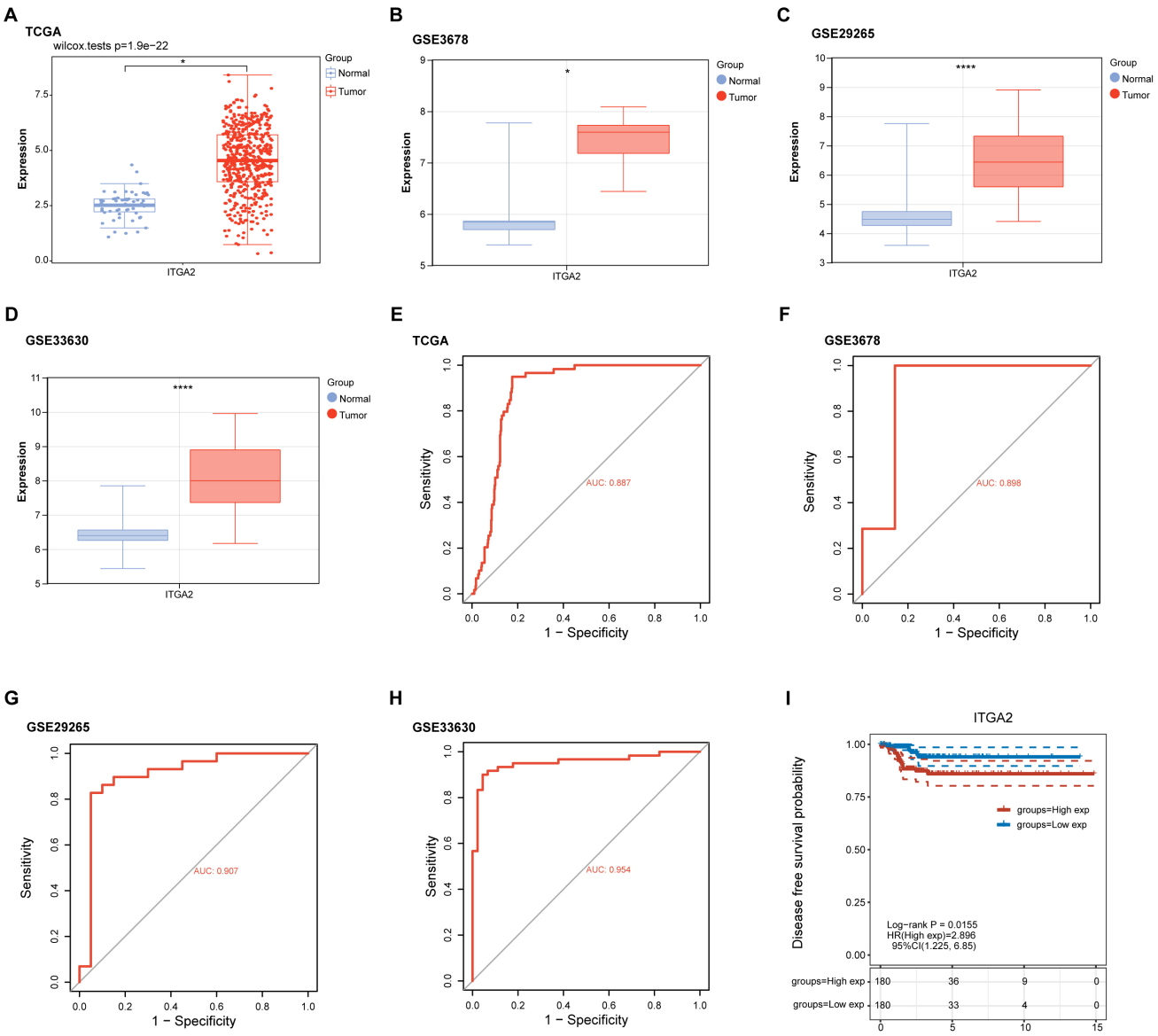

Fig. 4. Analysis of *ITGA2* expression and diagnostic performance. (A–D) *ITGA2* expression level in tumor and control samples from the TCGA-THCA, GSE3678, GSE29265, and GSE33630 datasets. Red dots represent tumor samples, and blue dots represent normal samples. *$p < 0.05$, ****$p < 0.001$. (E–H) Diagnostic performance of *ITGA2* expression as assessed by ROC curves across the same datasets. (I) KM survival curves reveal a significant association between ITGA2 gene expression levels and disease-free survival in thyroid cancer patients. The red solid line indicates the high expression group and the blue dashed line indicates the low expression group. *p*-value was 0.0155; HR was 2.896, 95% CI 1.225 to 6.85. TCGA-THCA, The Cancer Genome Atlas Thyroid Carcinoma; GSE3678, GSE29265, GSE33630, Gene Expression Omnibus dataset identifiers; AUC, Area Under the Curve; ROC, Receiver Operating Characteristic; KM, Kaplan-Meier; HR, Hazard Ratio; CI, confidence intervals.

tion curves further validated the predictive accuracy of the model, showing good agreement between the predicted 1-, 3-, and 5-year survival probabilities and the actual observations (Fig. 3D). Notably, most of the actual observations in Fig. 3D are clustered near the upper-right corner, which reflects the overall high survival probability in the TC cohort. The expression level of the *ITGA2* gene was significantly correlated with the prognosis of patients with thyroid cancer.

3.4 Up-regulation of ITGA2 Gene Expression in Thyroid Cancer and Evaluation of its Diagnostic Potential

In this study, we analyzed the expression pattern of the *ITGA2* gene in thyroid cancer and its potential as a diagnostic marker. The volcano map show that the expression level of *ITGA2* was significantly up-regulated in tumor samples compared to normal samples in the TCGA database (Fig. 4A). In addition, box line plots revealed that the expression levels of *ITGA2* were significantly

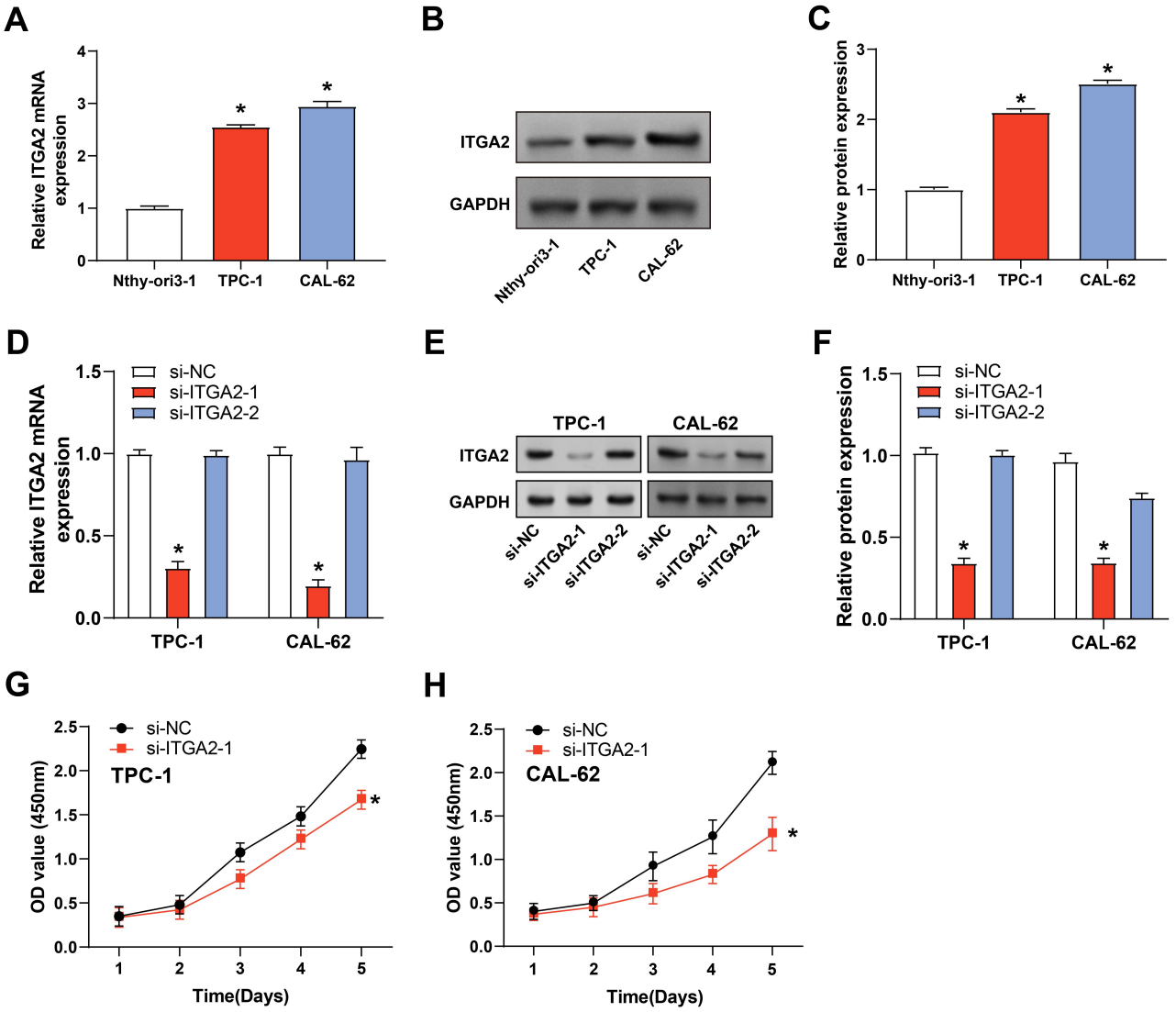

Fig. 5. Validation of *ITGA2* knockdown and its impact on TC cell viability. (A–C) Relative mRNA (A) and protein (B,C) expression levels of *ITGA2* in Nthy-ori3-1, TPC-1, and CAL-62 cell lines. Data are normalized to GAPDH and expressed as fold change relative to control. (D–F) Confirmation of si-*ITGA2*-1 knockdown efficacy in TC cells via qRT-PCR and WB. Results were normalized to GAPDH and presented as fold changes relative to the si-NC (n = 3 for each group). (G,H) CCK-8 demonstrated reduced cell proliferation over a 5-day period in TC cells following *ITGA2* knockdown. The absorbance at 450 nm (OD value) was measured to assess cell viability. Three independent experiments present Data as mean ± SD (n = 3). qRT-PCR, quantitative Real-Time Polymerase Chain Reaction; WB, Western Blot; si-NC, non-targeting control siRNA; CCK-8, Cell Counting Kit-8; OD, Optical Density. "*" indicates $p < 0.05$ compared to the si-NC.

higher in tumor samples than in normal samples in the GSE3678, GSE29265, and GSE33630 datasets, especially in the GSE29265 and GSE33630 datasets (Fig. 4B–D). Further, ROC curve analysis was performed to evaluate the potential of *ITGA2* gene expression as a diagnostic marker (Fig. 4E–H). The results showed that the AUC value of *ITGA2* was as high as 0.887 in the TCGA dataset, indicating a very high diagnostic accuracy. In the GSE3678 and GSE33630 datasets, the AUC values of *ITGA2* were 0.898 and 0.954, respectively, which also showed good diagnostic performance. The AUC value of *ITGA2* in the GSE29265 dataset was 0.907, further confirming its potential as a diagnostic marker. We analyzed the effect of *ITGA2* gene expression on disease-free survival in patients using the TCGA dataset. Analysis of the Clinical BioLetter House platform (n = 512) showed that high *ITGA2* expression was significantly associated with lower disease-free survival (Fig. 4I), a finding supported by results from the GEPIA database (n = 500) (**Supplementary Fig. 2A**). However, no significant association between *ITGA2* expression and disease-free survival was found when the TCGA dataset (n = 497) was analyzed by the cBioPortal

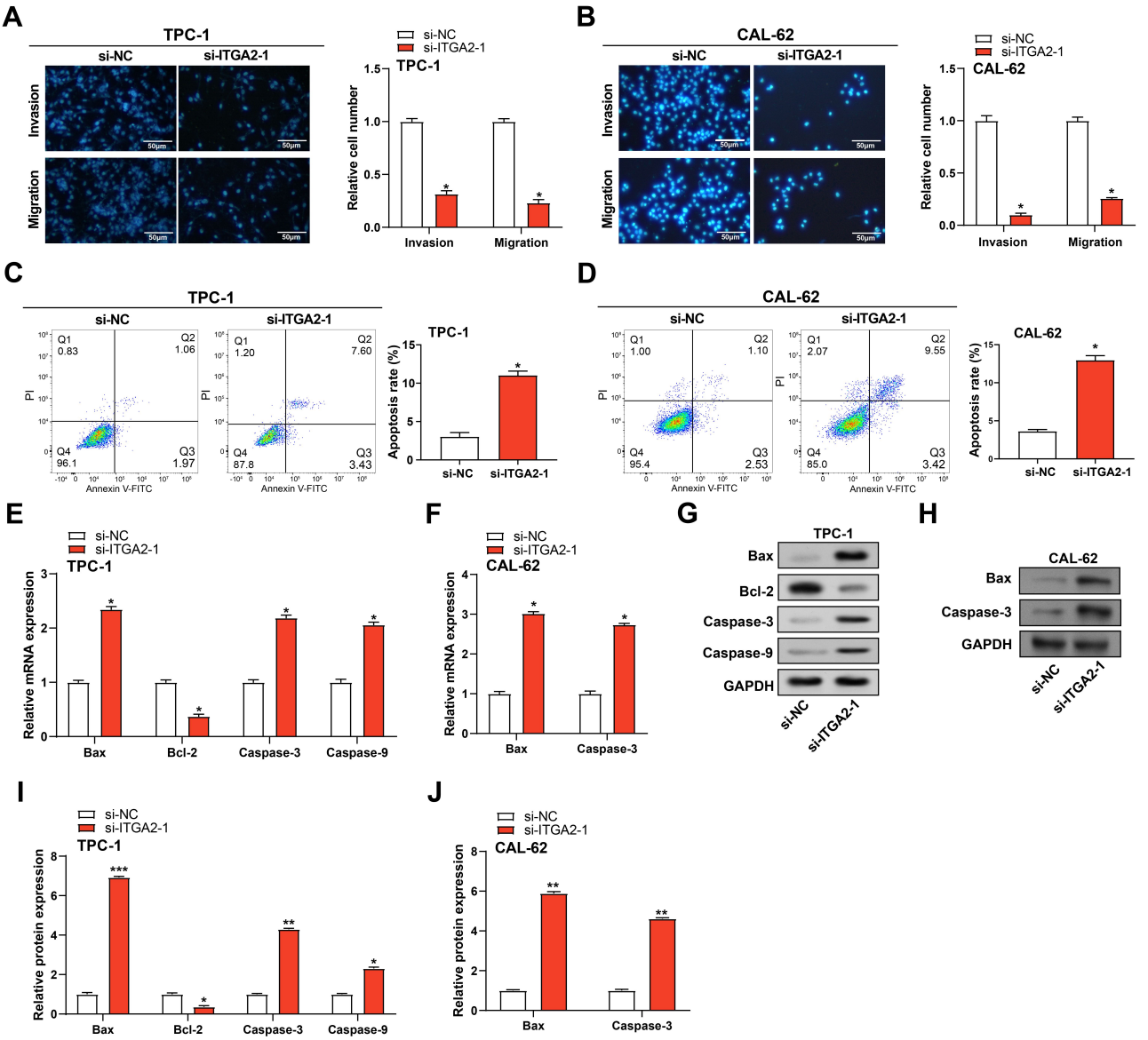

Fig. 6. Impact of *ITGA2* knockdown on cell behavior in TC cell. (A,B) Transwell test data demonstrating the effect of *ITGA2* knockdown on the migratory and invasion capacities of TC cells (n = 3 per group). The bar graph represents the average number of cells that migrated or invaded through the membrane. Scale bar, 50 µm. (C,D) Flow cytometry analysis of apoptosis rates in TC cells following *ITGA2* knockdown (n = 3 per group). The left panel shows flow cytometry plots, and the right panel presents a quantitative analysis of the results. (E–J) qRT-PCR and WB were used to detect changes in mRNA and protein expression of apoptosis-related genes (*Bax*, *Bcl-2*, *caspase3*, and *caspase9*) in TPC-1 cells after knockdown of *ITGA2*, and changes in mRNA and protein expression of Bax and caspase3 in CAL-62 cells (n = 3 per group). GAPDH was used as a loading control and was expressed as fold change relative to si-NC. si-NC, non-targeting control siRNA; qRT-PCR, quantitative Real-Time Polymerase Chain Reaction; WB, Western Blot. "*", "**", and "***" indicate $p < 0.05$, $p < 0.01$, and $p < 0.001$, respectively, compared to the si-NC.

platform (**Supplementary Fig. 2B**). Different analytical methods or platform differences may cause this discrepancy.

3.5 ITGA2 is Highly Expressed in TC Cell Lines and Affects Cell Viability

qRT-PCR and WB methods were used to investigate *ITGA2* expression in TC cell lines TPC-1 and CAL-62, and normal thyroid cells (Nthy-ori3-1). Significant up-regulation of *ITGA2* expression was observed in TC cell lines (Fig. 5A–C). Further, qRT-PCR and WB assays confirmed the efficient knockdown of *ITGA2* by si-*ITGA2*-1 in TC cell lines (Fig. 5D–F). Cell viability declined significantly following *ITGA2* knockdown in TC cell lines, as shown by the CCK-8 assay (Fig. 5G,H). Therefore, changes in ITGA2 expression were associated with altered biolog-

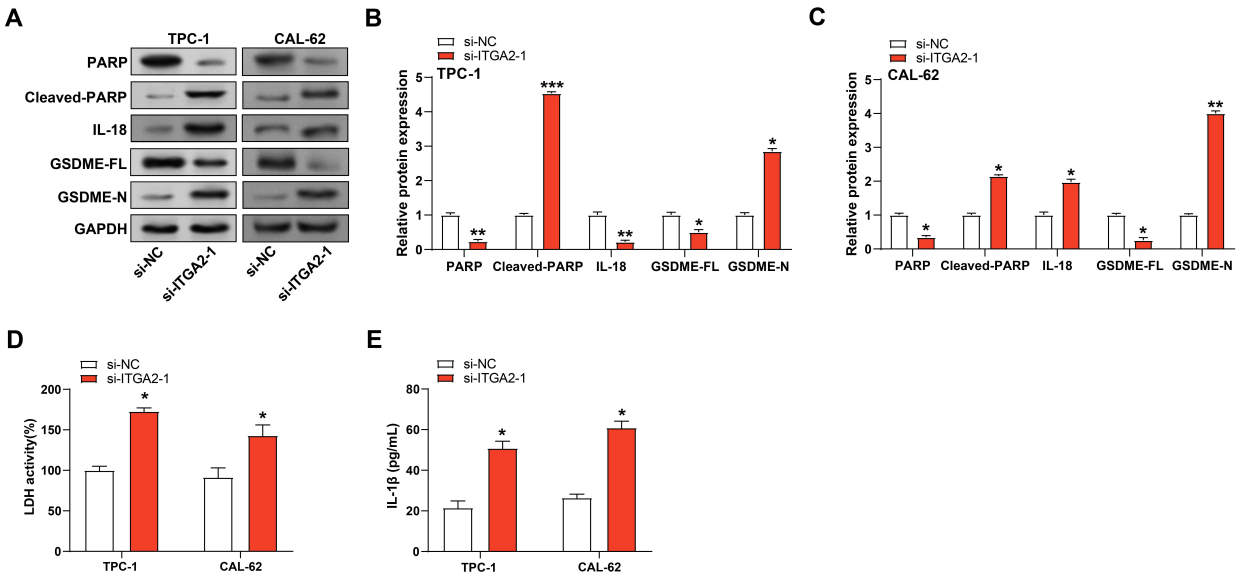

Fig. 7. *ITGA2* knockdown induces apoptosis and pyroptosis in TC cells. (A–C) qPCR and WB were performed to detect changes in mRNA and protein expression levels of apoptotic proteins (PARP and cleaved-PARP), pro-inflammatory cytokines IL-18 and pyroptotic proteins (GSDME-FL and GSDME-N) in TC cells after knockdown of *ITGA2* (n = 3 per group). GAPDH was used as a loading control. (D) LDH activity assay showing changes in cell membrane integrity and cytotoxicity in TC cells after *ITGA2* knockdown. The bar graph represents the mean LDH level (n = 3 per group). (E) ELISA measuring IL-1β secretion from TC cells after *ITGA2* knockdown. The bar graph shows the mean IL-1β concentration (n = 3 per group), reflecting the inflammatory response under different treatment conditions. si-NC, non-targeting control siRNA; WB, Western Blot; LDH, Lactate dehydrogenase; ELISA, Enzyme-linked immunosorbent assay. "*", "**", and "***" indicate $p < 0.05$, $p < 0.01$, and $p < 0.001$, respectively, compared to the si-NC.

ical behavior in TC cells, further supporting the important role of this key gene.

3.6 ITGA2 Knockdown Inhibits the Growth of TC Cells and Induces Apoptosis

Transwell tests demonstrated that *ITGA2* knockdown dramatically decreased the TC cells' migration and invasion capacity (Fig. 6A,B). Flow cytometry analysis also demonstrated a marked increase in the apoptosis rate of TC cells with silenced *ITGA2* (Fig. 6C,D). qRT-PCR analysis showed that *ITGA2* knockdown in TPC-1 cells led to up-regulation of the pro-apoptotic genes *Caspase-3*, *Bax*, and *Caspase-9* and down-regulation of the anti-apoptotic gene *Bcl-2* (Fig. 6E). This was further confirmed at the protein level by WB analysis. Cells with *ITGA2* knockdown showed significantly reduced expression of anti-apoptotic proteins relative to the control group but increased expression of a pro-apoptotic marker (Fig. 6G,I). In CAL-62 cells, *ITGA2* knockdown resulted in a significant up-regulation of Caspase-3 and Bax expression, whereas the changes in Bcl-2 and Caspase-9 expression were not significant compared with the control (Fig. 6F,H,J). This suggests that in CAL-62 cells, *ITGA2* knockdown may promote apoptosis mainly by affecting Caspase-3 and Bax, but not through the Bcl-2 and Caspase-9 pathways. We hypothesize that this difference may reflect the diversity of responses to *ITGA2* knockdown in different thyroid cancer cell lines or suggest that CAL-62 cells may be more dependent on the Caspase-3 and Bax-mediated apoptotic pathways.

3.7 ITGA2 Knockdown in TC Cells Induces Pyroptosis and Inflammation

WB analysis showed that the expression of proteins related to apoptosis, pro-inflammatory cytokines and pyroptosis was significantly changed in TC cell lines after *ITGA2* knockdown. Specifically, the full-length (FL) forms of PARP and GSDME were reduced. In contrast, the cleaved forms (cleaved-PARP and GSDME-N), as well as the pro-inflammatory cytokine IL-18, were significantly up-regulated in the si-ITGA2-1 group as compared to the control group (Fig. 7A–C). In addition, LDH activity in TC cells was notably increased after *ITGA2* knockdown, indicating increased cytotoxicity (Fig. 7D). ELISA assay also showed that IL-1β levels were significantly higher in si-*ITGA2*-1-treated cells compared to the control group (Fig. 7E). These results indicate that *ITGA2* knockdown in TC cells induces pyroptosis and promotes inflammatory responses.

3.8 Knockdown of ITGA2 in TC Cells Increases DNA Damage Response and ROS Generation

WB analysis revealed that *ITGA2* knockdown significantly upregulated the expression of key DNA damage response markers (γ-H2AX, p-CHK2, and p-ATM) compared

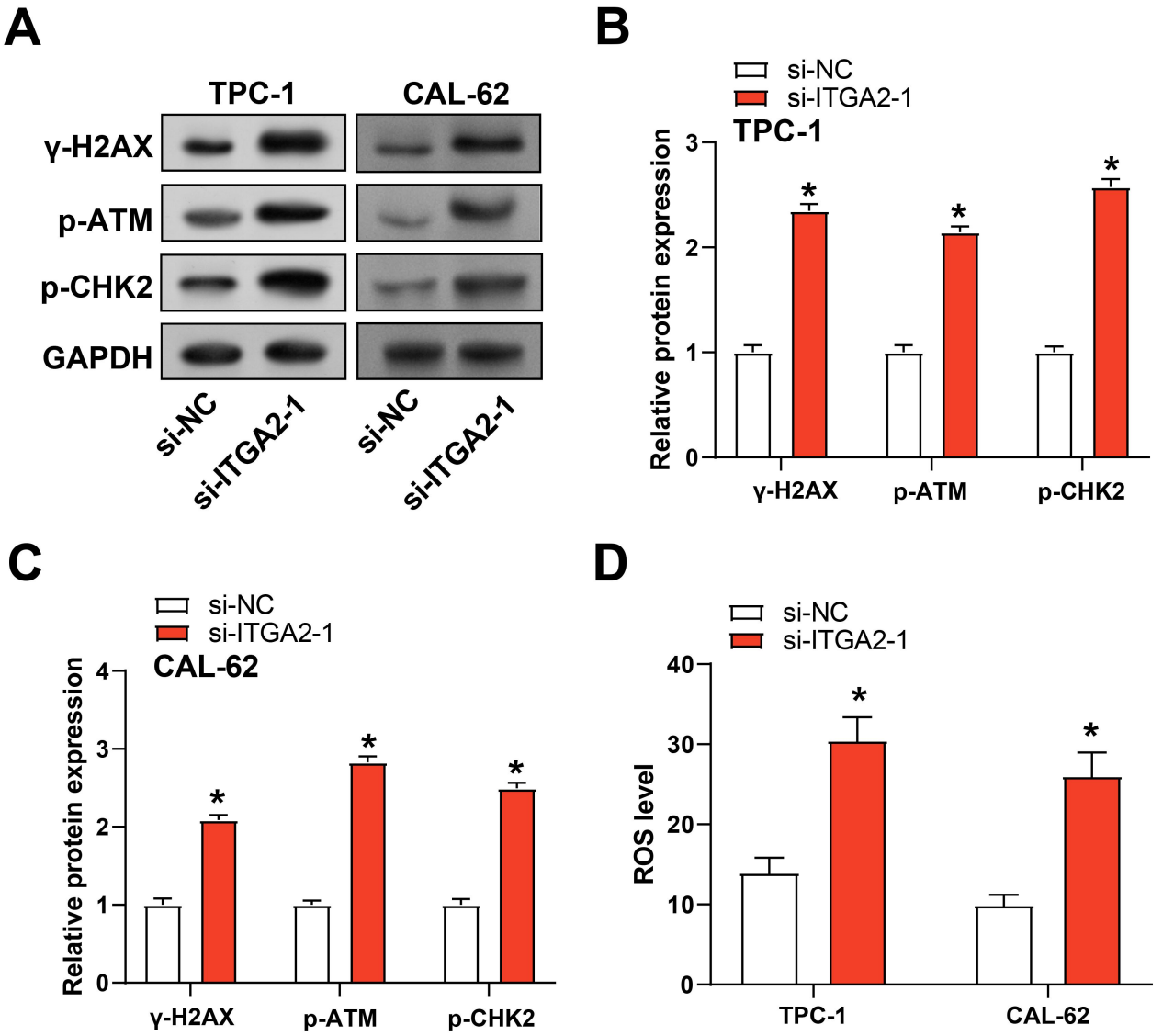

Fig. 8. *ITGA2* knockdown induces DNA damage and ROS production in TC cells. (A–C) WB analysis of DNA damage-related protein expression (phosphorylated ataxia telangiectasia mutated (p-ATM), phosphorylated histone H2AX on serine 139 (γ-H2AX), and phosphorylated checkpoint kinase 2 (p-CHK2)) in TC cells after *ITGA2* knockdown (n = 3 per group). GAPDH was used as a loading control and presented as fold-changes compared to the si-NC. (D) Measurement of ROS levels in TC cells following *ITGA2* knockdown using a ROS detection kit (n = 3 per group). The bar graph represents the mean fluorescence intensity, indicating ROS production under different treatment conditions. si-NC, non-targeting control siRNA; WB, Western Blot; ROS, reactive oxygen species. "*" indicates $p < 0.05$ compared to the si-NC.

to the si-NC control (Fig. 8A–C). Additionally, *ITGA2* knockdown caused ROS to increase significantly in TC cell lines, as measured by the fluorescence intensity (Fig. 8D). These findings indicate that *ITGA2* knockdown induces DNA damage and oxidative stress in TC cells.

3.9 Knockdown of ITGA2 Inhibits TC Stemness by Suppressing the Wnt/β-catenin Pathway and Suppresses Tumor Growth In Vivo

qRT-PCR analysis revealed that *ITGA2* knockdown in TC cells markedly decreased the expression of genes associated with the Wnt/β-catenin signaling pathway, such as snail, c-Myc, CD44, Wnt-1, slug, and β-catenin (Fig. 9A,B). WB assays further confirmed the down-regulation of these genes at the protein level (Fig. 9C–E), suggesting that *ITGA2* knockdown inhibits stemness in TC cells by impeding the Wnt/β-catenin signaling pathway. *In vivo,* tumorigenesis assays were performed by injecting si-*ITGA2*-1-transfected TPC-1 cells into the flanks of mice. After four weeks, the *ITGA2* knockdown group's tumor weight and volume were noticeably lower than those of the control group (Fig. 10A–C). ITGA2 is localized in the cy-

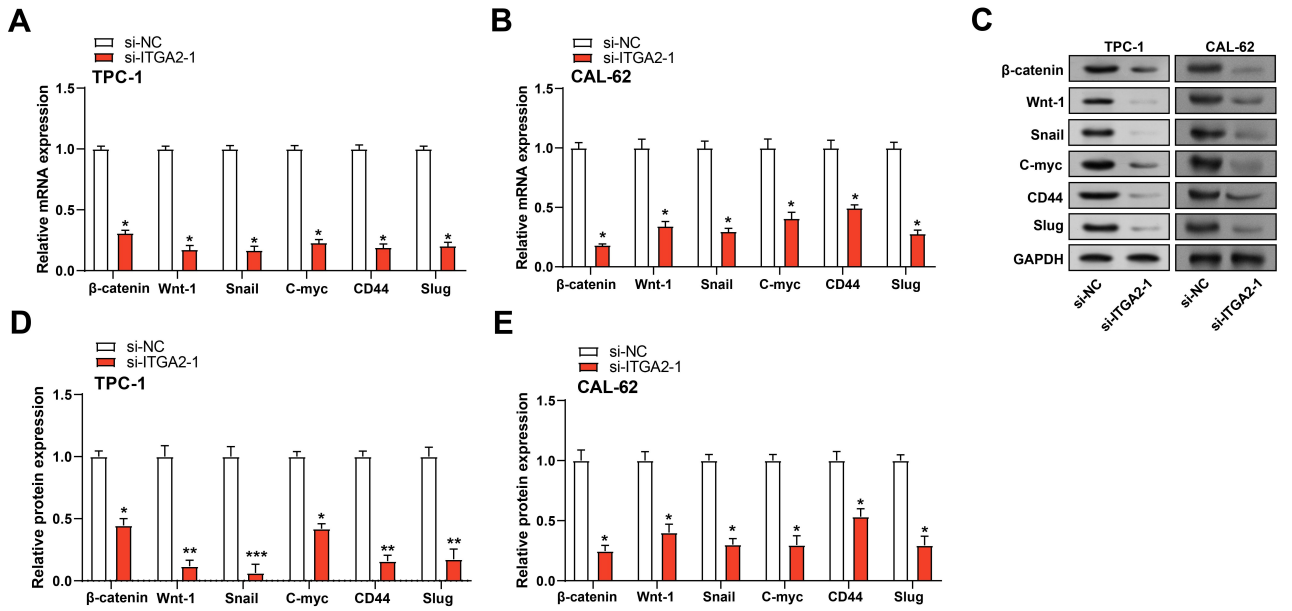

Fig. 9. Knockdown of *ITGA2* inhibits TC stemness by suppressing the Wnt/β-catenin signaling pathway. (A–E) qRT-PCR and WB analysis of mRNA and protein expression levels of β-catenin, Wnt-1, Snail, C-myc, CD44, and Slug in TC cells after *ITGA2* knockdown (n = 3 per group). GAPDH was used as a loading control, presented as fold-changes relative to the si-NC. si-NC, non-targeting control siRNA; qRT-PCR, quantitative Real-Time Polymerase Chain Reaction; WB, Western Blot. "*", "**", and "***" indicate $p < 0.05$, $p < 0.01$, and $p < 0.001$, respectively, compared to the si-NC.

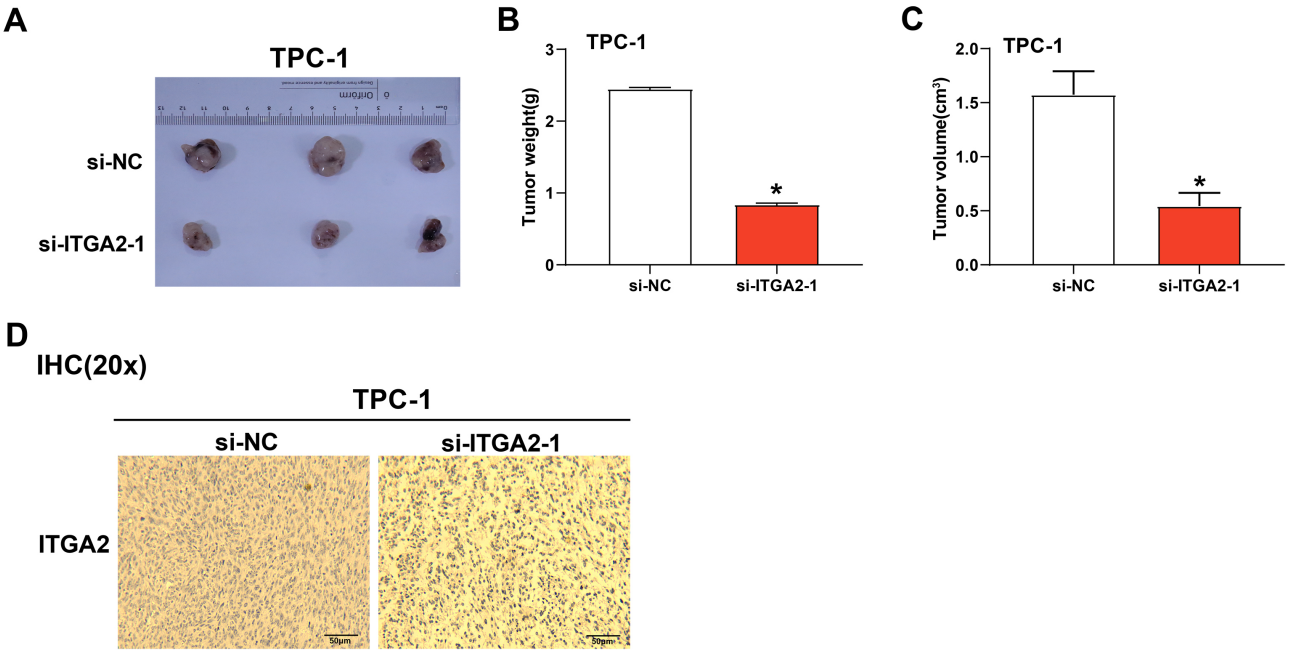

Fig. 10. *ITGA2* knockdown reduced tumor growth *in vivo*. (A) Representative images of tumors harvested from nude mice bearing TPC-1 cells transfected with either si-NC or si-*ITGA2*-1 (n = 3 per group). (B) Bar graph showing tumor weights in mice injected with TPC-1 cells transfected with si-NC or si-*ITGA2*-1 (n = 5 per group). (C) Bar graph displaying tumor volumes in mice injected with TPC-1 cells transfected with si-NC or si-*ITGA2*-1 (n = 5 per group). (D) IHC analysis of ITGA2 expression in tumor sections from the *in vivo* tumorigenesis assay (n = 5 per group). Scale bar, 50 µm. si-NC, non-targeting control siRNA; IHC, Immunohistochemistry; Nude mice, immunodeficient mice. "*" indicates $p < 0.05$ compared to the si-NC.

toplasm, the, immunohistochemical analysis further confirmed that *ITGA2* expression was down-regulated in tumors from the *ITGA2* knockdown group (Fig. 10D).

4. Discussion

With a rising prevalence globally, TC is the most common endocrine cancer. The most common kind of TC, papillary thyroid carcinoma (PTC), has few effective treatment options for advanced or metastatic TC, despite advancements in screening and therapy. The discovery of novel therapy targets and prognostic indicators is therefore essential for improving patient survival. Through a bioinformatics analysis of the TCGA-THCA, GSE3678, GSE29265, and GSE33630 datasets, the present study identified three crucial prognostic genes in TC: *EFEMP1*, *EGR2*, and *ITGA2*. *EGR2* has become one of the most critical tumor suppressor genes in PTC. Qiu *et al*. [23] reported that *EGR2* shows elevated transcriptional activity in PTC tissues in comparison with normal controls, and is involved in regulating the cell cycle and degradation of the extracellular matrix. *EFEMP1* was also identified as another critical player in the progression of PTC. Li *et al*. [24] reported that *EFEMP1* was a hub protein involved in tumor development, with its upregulation correlating with disease progression. The significant expression of *EFEMP1* in PTC tissues indicates that it may serve as a target for therapy. Finally, our nomogram analysis identified *ITGA2* as a hub gene in TC. Expression analysis confirmed that *ITGA2* was significantly overexpressed in tumor samples from the TCGA-THCA, GSE3678, GSE29265, and GSE33630 datasets, thus supporting a role in TC progression. *ITGA2* is a transmembrane receptor involved in cell adhesion and migration. As such, it is a potential target for upcoming treatment approaches and may aid in tumor invasion and metastasis.

Apoptosis and pyroptosis represent two different types of programmed cell death. Apoptosis involves the caspase-3, Bax, Bcl-2, and caspase-9 proteins, which control mitochondrial permeability and initiate the cell death cascade [25]. Additionally, cleaved-PARP plays a critical role in DNA degradation during apoptosis [26]. In contrast, pyroptosis is driven by gastrin proteins, particularly GSDME. These form membrane pores, leading to inflammatory cell death [27]. While apoptosis typically maintains cellular homeostasis, pyroptosis triggers a robust immune response due to its inflammatory nature [28]. Several studies have shown that both apoptotic and pyroptotic pathways can influence tumor progression in TC. For example, Zhou J *et al*. [29] showed that naringin promotes apoptosis by simultaneously increasing the levels of caspase-3, Bax, and cleaved-caspase-3, while decreasing the levels of anti-apoptotic proteins such as Bcl-2. Similarly, Zhou X *et al*. [30] discovered that downregulating *SPTBN2* causes cell cycle arrest by increasing the expression of cleaved caspase-3 and Bax and decreasing that of Bcl-2, which results in apoptosis. Importantly, Hu *et al*. [31] demonstrated that Alantolactone triggers GSDME-dependent pyroptosis and apoptosis in anaplastic TC, thus highlighting the dual role of cell death pathways in tumor suppression. The present study further highlights the importance of pyroptosis in TC. We observed that silencing of *ITGA2* inhibited cell growth and simultaneously induced apoptosis. Moreover, *ITGA2* knockdown induced pyroptosis, as seen by elevated levels of cleaved-GSDME, LDH and IL-1β release. This was accompanied by a notable decrease in pro-survival proteins such as PARP and GSDME-FL. Our findings implicate *ITGA2* in pyroptosis and apoptosis, suggesting it may be a possible therapeutic target in TC, particularly for strategies that induce pyroptosis.

DNA damage is a critical event that can lead to genomic instability and promote cancer development. It initiates a cellular response involving essential proteins such as γ-H2AX, p-CHK2, and p-ATM [32]. γ-H2AX marks DNA double-strand breaks, thus serving as an early signal for repair processes [33]. ATM kinase phosphorylates substrates like CHK2, thereby activating DNA repair pathways and inducing cell cycle arrest [34]. When these mechanisms fail or are overwhelmed, the damaged cells may evade repair and proliferate uncontrollably, contributing to tumorigenesis. The regulation of DNA damage response proteins is therefore essential for preventing cancer progression and maintaining genomic integrity. Several previous investigations have focused on the function of DNA damage in TC. Xu *et al*. [35] showed that *YM155* induced significant DNA damage in ATC through oxidative stress. This was marked by increased γ-H2AX, causing apoptosis and cell cycle arrest. Similarly, Wu *et al*. [36] demonstrated that paclitaxel (PTX) combined with recombinant adenovirus-p53 increased DNA damage in PTC. This resulted in elevated p-ATM and γ-H2AX levels, thereby improving the anti-tumor efficacy of PTX. Furthermore, Wang *et al*. [37] reported that inhibition of *SGLT2* by canagliflozin induced DNA damage via activation of the ATM/CHK2 pathway, resulting in G1/S phase arrest and increased apoptosis. Our findings support these observations, as *ITGA2* knockdown in TC cells significantly increased the levels of DNA damage indicators, including γ-H2AX, p-ATM, and p-CHK2. Additionally, the silencing of *ITGA2* resulted in elevated ROS levels, indicating that oxidative stress contributes to the enhanced DNA damage response. These findings underline the role of ITGA2 in DNA damage repair as well as highlight its possible use as a therapeutic target for enhancing DNA damage-induced cancer cell death.

Cell migration and proliferation are regulated by the Wnt/β-catenin signaling system. Wnt proteins, including Wnt-1, bind to Frizzled receptors, causing β-catenin to stabilize and aggregate in the cytoplasm [38]. After stabilizing, β-catenin moves to the nucleus, where it attaches itself to T cell factor/lymphoid enhancer-binding factor (TCF/LEF) transcription factors and activates target genes

that are involved in cell adhesion and proliferation, including *CD44* and *C-myc* [39]. Additionally, β-catenin affects the expression of other transcription factors, including snail and slug, which are necessary for epithelial-mesenchymal transition (EMT) and, consequently, the facilitation of invasion and migration of cells [17]. TC is one of the several cancer forms that are frequently associated with dysregulation of this system. Gilbert-Sirieix *et al*. [40] shown that the Wnt/β-catenin pathway influences the course of PTC by upregulating *TTF-1* expression. Zhang *et al*. [41] demonstrated that miR-200c affects the Wnt/β-catenin signaling cascade by targeting parathyroid hormone-like hormone (PTHLH) and modulating the growth, and EMT of ATC cells. Our research showed that *ITGA2* knockdown leads to significantly reduced expression of CD44, C-myc, Wnt-1, slug, snail, and β-catenin in TC cells, as well as markedly lower tumor weight and volume in a xenograft model. These results imply that *ITGA2* is essential for regulating tumor development and the Wnt/β-catenin signaling pathway.

In the discussion section of this study, we first need to address a key issue: the differences in the results of the analysis of the relationship between *ITGA2* expression and disease-free survival in thyroid cancer patients by different analytical platforms. While the Clinical BioLetter House platform analysis showed that high *ITGA2* expression was significantly associated with lower disease-free survival, the cBioPortal platform did not find a significant association between *ITGA2* expression and disease-free survival when analyzed. This discrepancy could be due to several factors, including differences in analysis methods or platform-specific biases. This finding suggests that we must consider the effects of differences in analytical techniques and platforms when interpreting bioinformatics data.

Furthermore, the role of *ITGA2* in thyroid cancer cells may be more complex than previously thought. Our results suggest that *ITGA2* may play a role in multiple cell death pathways, not only apoptosis. Although WB experiments showed significant changes in the levels of apoptosis-related markers after *ITGA2* inhibition, the increase in apoptosis rate was not as substantial as expected. This suggests that *ITGA2* may regulate the apoptotic process by affecting multiple signaling pathways rather than direct induction. In addition, we observed that *ITGA2* inhibition may involve other types of cell death, such as pyroptosis, which may somewhat mask the increase in apoptosis.

ITGA2 may play different roles in different biological contexts. In some cases, *ITGA2* may promote tumor growth primarily by inhibiting apoptosis, whereas in others, it may act through mechanisms such as promoting cell migration or angiogenesis. Our findings highlight the multifaceted nature of *ITGA2* in thyroid cancer and the multiple biological processes that may be involved in tumor progression. These findings provide new directions for future studies, including further exploration of the specific mechanisms of *ITGA2* in apoptosis regulation and how *ITGA2* interacts with other cell death pathways.

In summary, our findings suggest that *ITGA2* may play a role in multiple cell death pathways and emphasize the importance of considering differences in analysis methods and platforms when interpreting bioinformatics data. Future studies should include cross-platform data validation and in-depth biological mechanism studies to ensure the accuracy and clinical relevance of the findings.

5. Conclusion

This study emphasizes the importance of *ITGA2* in the development of TC, as well as its potential as a therapy target. *ITGA2* knockdown reduced TC cell viability, migration, as well as the promotion of apoptosis and pyroptosis. Furthermore, *ITGA2* silencing enhanced the DNA damage response and increased ROS production, contributing to elevated cellular stress. *ITGA2* knockdown also repressed the Wnt/β-catenin signaling pathway resulting in reduced cancer stemness, as demonstrated by decreased tumor growth *in vivo*. These results imply that *ITGA2* could be a viable treatment target for the induction of DNA damage and pyroptosis in TC cells, as well as for the disruption of stemness.

Availability of Data and Materials

The datasets used and analyzed during the current study are available from the corresponding authors upon reasonable request.

Author Contributions

Conception and design of the research: LY, DMH, RY, ZLL, and YF. Acquisition of data: LY, DMH, and RY. Analysis and interpretation of data: LY, DMH, RY, JJ, and XSL. Statistical analysis: XSL. Drafting the manuscript: LY, DMH, and RY. Revision of manuscript for important intellectual content: ZLL and YF. All authors contributed to editorial changes in the manuscript. All authors read and approved the final manuscript. All authors have participated sufficiently in the work and agreed to be accountable for all aspects of the work.

Ethics Approval and Consent to Participate

Our study is supported by the Animal Welfare and Ethics Committee of the Laboratory Animal Science Department, Fudan University (No. 2024-MHYY-304). All animal experiments were conducted in accordance with the institutional ethical guidelines and complied with the 3R (Replacement, Reduction, Refinement) principles.

Acknowledgment

Not applicable.

Funding

This study was funded by 2024 National Traditional Chinese Medicine Comprehensive Reform Pilot Zone "Advanced Talents in Integrated Traditional Chinese and Western Medicine" Project, Project Number: PDZY-2024-0708.

Conflict of Interest

The authors declare no conflict of interest.

Declaration of AI and AI-Assisted Technologies in the Writing Process

During the preparation of this work the authors used ChatGPT in order to check spell and grammar. After using this tool, the authors reviewed and edited the language of the Introduction and Discussion sections as needed and take full responsibility for the content of the publication.

Supplementary Material

Supplementary material associated with this article can be found, in the online version, at https://doi.org/10.31083/FBL27946.

References

[1] Deng Y, Li H, Wang M, Li N, Tian T, Wu Y, *et al*. Global Burden of Thyroid Cancer From 1990 to 2017. JAMA Network Open. 2020; 3: e208759. https://doi.org/10.1001/jamanetworkopen.2020.8759.

[2] Kim KJ, Song JE, Kim JY, Bae JH, Kim NH, Yoo HJ, *et al*. Effects of radioactive iodine treatment on cardiovascular disease in thyroid cancer patients: a nationwide cohort study. Annals of Translational Medicine. 2020; 8: 1235. https://doi.org/10.21037/atm-20-5222.

[3] Yin L, Luo X, Zhang X, Cheng B. The evolving process of ferroptosis in thyroid cancer: Novel mechanisms and opportunities. Journal of Cellular and Molecular Medicine. 2024; 28: e18587. https://doi.org/10.1111/jcmm.18587.

[4] D'Arcy MS. Cell death: a review of the major forms of apoptosis, necrosis and autophagy. Cell Biology International. 2019; 43: 582–592. https://doi.org/10.1002/cbin.11137.

[5] Hurtado-Navarro L, Angosto-Bazarra D, Pelegrín P, Baroja-Mazo A, Cuevas S. NLRP3 Inflammasome and Pyroptosis in Liver Pathophysiology: The Emerging Relevance of Nrf2 Inducers. Antioxidants (Basel, Switzerland). 2022; 11: 870. https://doi.org/10.3390/antiox11050870.

[6] Schumacher B, Pothof J, Vijg J, Hoeijmakers JHJ. The central role of DNA damage in the ageing process. Nature. 2021; 592: 695–703. https://doi.org/10.1038/s41586-021-03307-7.

[7] Tian Y, Dong J, Li L. Bridging Pyroptosis and Immunity: A Comprehensive Study of the Pyroptosis-Related Long Non-Coding RNA Signature in Breast Cancer. Life (Basel, Switzerland). 2023; 13: 1599. https://doi.org/10.3390/life13071599.

[8] Gregori A, Bergonzini C, Capula M, Mantini G, Khojasteh-Leylakoohi F, Comandatore A, *et al*. Prognostic Significance of Integrin Subunit Alpha 2 (ITGA2) and Role of Mechanical Cues in Resistance to Gemcitabine in Pancreatic Ductal Adenocarcinoma (PDAC). Cancers. 2023; 15: 628. https://doi.org/10.3390/cancers15030628.

[9] Kareddula A, Medina DJ, Petrosky W, Dolfi S, Tereshchenko I, Walton K, *et al*. The role of chromodomain helicase DNA binding protein 1 (CHD1) in promoting an invasive prostate cancer phenotype. Therapeutic Advances in Urology. 2021; 13: 17562872211022462. https://doi.org/10.1177/17562872211022462.

[10] Zhou C, Li S, Bin K, Qin G, Pan P, Ren D, *et al*. ITGA2 overexpression inhibits DNA repair and confers sensitivity to radiotherapies in pancreatic cancer. Cancer Letters. 2022; 547: 215855. https://doi.org/10.1016/j.canlet.2022.215855.

[11] Hu L, Chen W, Qian A, Li YP. Wnt/β-catenin signaling components and mechanisms in bone formation, homeostasis, and disease. Bone Research. 2024; 12: 39. https://doi.org/10.1038/s41413-024-00342-8.

[12] Liu J, Xiao Q, Xiao J, Niu C, Li Y, Zhang X, *et al*. Wnt/β-catenin signalling: function, biological mechanisms, and therapeutic opportunities. Signal Transduction and Targeted Therapy. 2022; 7: 3. https://doi.org/10.1038/s41392-021-00762-6.

[13] Wang J, Tian Y, Chen H, Li H, Zheng S. Key signaling pathways, genes and transcription factors associated with hepatocellular carcinoma. Molecular Medicine Reports. 2018; 17: 8153–8160. https://doi.org/10.3892/mmr.2018.8871.

[14] Liang L, Li Y, Ying B, Huang X, Liao S, Yang J, *et al*. Mutation-associated transcripts reconstruct the prognostic features of oral tongue squamous cell carcinoma. International Journal of Oral Science. 2023; 15: 1. https://doi.org/10.1038/s41368-022-00210-3.

[15] Agarwal JR, Griesinger F, Stühmer W, Pardo LA. The potassium channel Ether à go-go is a novel prognostic factor with functional relevance in acute myeloid leukemia. Molecular Cancer. 2010; 9: 18. https://doi.org/10.1186/1476-4598-9-18.

[16] Xie Y, Shi H, Han B. Bioinformatic analysis of underlying mechanisms of Kawasaki disease via Weighted Gene Correlation Network Analysis (WGCNA) and the Least Absolute Shrinkage and Selection Operator method (LASSO) regression model. BMC Pediatrics. 2023; 23: 90. https://doi.org/10.1186/s12887-023-03896-4.

[17] Xue W, Yang L, Chen C, Ashrafizadeh M, Tian Y, Sun R. Wnt/β-catenin-driven EMT regulation in human cancers. Cellular and Molecular Life Sciences: CMLS. 2024; 81: 79. https://doi.org/10.1007/s00018-023-05099-7.

[18] Koch DT, Yu H, Beirith I, Schirren M, Drefs M, Liu Y, *et al*. Tigecycline causes loss of cell viability mediated by mitochondrial OXPHOS and RAC1 in hepatocellular carcinoma cells. Journal of Translational Medicine. 2023; 21: 876. https://doi.org/10.1186/s12967-023-04615-4.

[19] Marfella R, Prattichizzo F, Sardu C, Paolisso P, D'Onofrio N, Scisciola L, *et al*. Evidence of an anti-inflammatory effect of PCSK9 inhibitors within the human atherosclerotic plaque. Atherosclerosis. 2023; 378: 117180. https://doi.org/10.1016/j.atherosclerosis.2023.06.971.

[20] Schweppe RE, Klopper JP, Korch C, Pugazhenthi U, Benezra M, Knauf JA, *et al*. Deoxyribonucleic acid profiling analysis of 40 human thyroid cancer cell lines reveals cross-contamination resulting in cell line redundancy and misidentification. The Journal of Clinical Endocrinology and Metabolism. 2008; 93: 4331–4341. https://doi.org/10.1210/jc.2008-1102.

[21] Xing M. Molecular pathogenesis and mechanisms of thyroid cancer. Nature Reviews. Cancer. 2013; 13: 184–199. https://doi.org/10.1038/nrc3431.

[22] Ma H, Bell KN, Loker RN. qPCR and qRT-PCR analysis: Regulatory points to consider when conducting biodistribution and vector shedding studies. Molecular Therapy. Methods & Clinical Development. 2020; 20: 152–168. https://doi.org/10.1016/j.omtm.2020.11.007.

[23] Qiu J, Zhang W, Xia Q, Liu F, Li L, Zhao S, *et al*. RNA sequencing identifies crucial genes in papillary thyroid carcinoma (PTC) progression. Experimental and Molecular Pathology. 2016; 100: 151–159. https://doi.org/10.1016/j.yexmp.2015.12.011.

[24] Li WB, Zhou J, Xu L, Su XL, Liu Q, Pang H. Identification

of Genes Associated with Papillary Thyroid Carcinoma (PTC) for Diagnosis by Integrated Analysis. Hormone and Metabolic Research = Hormon- Und Stoffwechselforschung = Hormones et Metabolisme. 2016; 48: 226–231. https://doi.org/10.1055/s-0035-1569289.

[25] Flores-Romero H, Dadsena S, García-Sáez AJ. Mitochondrial pores at the crossroad between cell death and inflammatory signaling. Molecular Cell. 2023; 83: 843–856. https://doi.org/10.1016/j.molcel.2023.02.021.

[26] Li Y, Tong Y, Liu J, Lou J. The Role of MicroRNA in DNA Damage Response. Frontiers in Genetics. 2022; 13: 850038. https://doi.org/10.3389/fgene.2022.850038.

[27] Xia S, Hollingsworth LR, 4th, Wu H. Mechanism and Regulation of Gasdermin-Mediated Cell Death. Cold Spring Harbor Perspectives in Biology. 2020; 12: a036400. https://doi.org/10.1101/cshperspect.a036400.

[28] Zheng Z, Li G. Mechanisms and Therapeutic Regulation of Pyroptosis in Inflammatory Diseases and Cancer. International Journal of Molecular Sciences. 2020; 21: 1456. https://doi.org/10.3390/ijms21041456.

[29] Zhou J, Xia L, Zhang Y. Naringin inhibits thyroid cancer cell proliferation and induces cell apoptosis through repressing PI3K/AKT pathway. Pathology, Research and Practice. 2019; 215: 152707. https://doi.org/10.1016/j.prp.2019.152707.

[30] Zhou X, Lin L, Qi Y, Xu M, Xu Q, Wang Y, *et al*. *SPTBN2* Promotes the Progression of Thyroid Cancer by Accelerating G1/S Transition and Inhibiting Apoptosis. Disease Markers. 2022; 2022: 2562595. https://doi.org/10.1155/2022/2562595.

[31] Hu Y, Wen Q, Cai Y, Liu Y, Ma W, Li Q, *et al*. Alantolactone induces concurrent apoptosis and GSDME-dependent pyroptosis of anaplastic thyroid cancer through ROS mitochondria-dependent caspase pathway. Phytomedicine: International Journal of Phytotherapy and Phytopharmacology. 2023; 108: 154528. https://doi.org/10.1016/j.phymed.2022.154528.

[32] Gachechiladze M, Skarda J, Bouchalova K, Soltermann A, Joerger M. Predictive and Prognostic Value of DNA Damage Response Associated Kinases in Solid Tumors. Frontiers in Oncology. 2020; 10: 581217. https://doi.org/10.3389/fonc.2020.581217.

[33] Katsuta E, Sawant Dessai A, Ebos JM, Yan L, Ouchi T, Takabe K. H2AX mRNA expression reflects DNA repair, cell proliferation, metastasis, and worse survival in breast cancer. American Journal of Cancer Research. 2022; 12: 793–804.

[34] Phan LM, Rezaeian AH. ATM: Main Features, Signaling Pathways, and Its Diverse Roles in DNA Damage Response, Tumor Suppression, and Cancer Development. Genes. 2021; 12: 845. https://doi.org/10.3390/genes12060845.

[35] Xu Q, Mackay RP, Xiao AY, Copland JA, Weinberger PM. Ym155 Induces Oxidative Stress-Mediated DNA Damage and Cell Cycle Arrest, and Causes Programmed Cell Death in Anaplastic Thyroid Cancer Cells. International Journal of Molecular Sciences. 2021; 22: 1961. https://doi.org/10.3390/ijms22041961.

[36] Wu W, Wei T, Li Z, Zhu J. p53-dependent apoptosis is essential for the antitumor effect of paclitaxel response to DNA damage in papillary thyroid carcinoma. International Journal of Medical Sciences. 2021; 18: 3197–3205. https://doi.org/10.7150/ijms.61944.

[37] Wang Y, Yang L, Mao L, Zhang L, Zhu Y, Xu Y, *et al*. SGLT2 inhibition restrains thyroid cancer growth via G1/S phase transition arrest and apoptosis mediated by DNA damage response signaling pathways. Cancer Cell International. 2022; 22: 74. https://doi.org/10.1186/s12935-022-02496-z.

[38] Tsukiyama T. New insights in ubiquitin-dependent Wnt receptor regulation in tumorigenesis. In Vitro Cellular & Developmental Biology. Animal. 2024; 60: 449–465. https://doi.org/10.1007/s11626-024-00855-w.

[39] Gajos-Michniewicz A, Czyz M. WNT/β-catenin signaling in hepatocellular carcinoma: The aberrant activation, pathogenic roles, and therapeutic opportunities. Genes & Diseases. 2023; 11: 727–746. https://doi.org/10.1016/j.gendis.2023.02.050.

[40] Gilbert-Sirieix M, Makoukji J, Kimura S, Talbot M, Caillou B, Massaad C, *et al*. Wnt/β-catenin signaling pathway is a direct enhancer of thyroid transcription factor-1 in human papillary thyroid carcinoma cells. PloS One. 2011; 6: e22280. https://doi.org/10.1371/journal.pone.0022280.

[41] Zhang Y, Duan Y, Wu C, Peng W, Chen W, Wang L, *et al*. MiR-200c regulates invasion, proliferation and EMT of anaplastic thyroid cancer cells by targeting parathyroid hormone like hormone. Growth Factors (Chur, Switzerland). 2022; 40: 175–185. https://doi.org/10.1080/08977194.2022.2108809.